TID-4500, UC-34
Physics

Lawrence Radiation Laboratory
UNIVERSITY OF CALIFORNIA
LIVERMORE
94550

UCRL-51045

CABLE SHIELDING FROM PHOTON SCATTERING FOR PINEX EXPERIMENTS

D. M. Buchla
T. L. Harper
J. K. Wobser

CABLE SHIELDING FROM PHOTON SCATTERING FOR PINEX EXPERIMENTS

Abstract

Gamma induced noise in coaxial signal cables transmitting prompt data on events containing a pinex (PInhole Neutron EXperiment) has caused loss of prompt data on a number of events. Monte Carlo calculations of photo transport outside the pinex pipe with and without internal pipe collimators have been made. These calculations have been used to determine the induced cable noise current. Recommended shielding arrangements to reduce the induced noise current to an acceptable level are given. In addition, time dependent buildup in the cables is described.

Introduction

On a number of events with prompt diagnostic measurements and pinex (PInhole Neutron EXperiments), gamma-induced noise in prompt diagnostic cables has caused the loss of some prompt diagnostic data. This study helps the diagnostic physicist define optimum requirements for shielding in two different geometries. The first geometry assumes a 9-5/8 in. diam drill pipe containing no collimators. The second geometry assumes a 13-3/8 in. diam drill pipe with Pb collimation at intervals along the pipe.

Figure 1 indicates how photon scattering from the pinex pipe induces noise in the signal cables. Since propagation velocity in a cable is less than the photon velocity traveling along the line-of-sight, the noise induced in the cable will appear before the main detector signal. Negative signal polarities for the cable noise have been observed. The time between the noise peak and the detector signal depend upon the cable propagation velocity and the location along the pipe where the photon scattering took place.

Scattering calculations were performed with the aid of SORS-G, a Monte Carlo photon transport code.[1] These calculations were checked experimentally with detectors located along the pinex pipe on a recent NTS event. With the aid of the calculational models and experimentally measured cable sensitivities, the current induced in a coaxial cable as a function of distance from the source per source photon per sec is given for both uncollimated and collimated geometries.

The induced noise current is a function of distance from the source and the time relation of signal and noise currents and signal-to-noise ratio must be considered to determine the required shielding. The

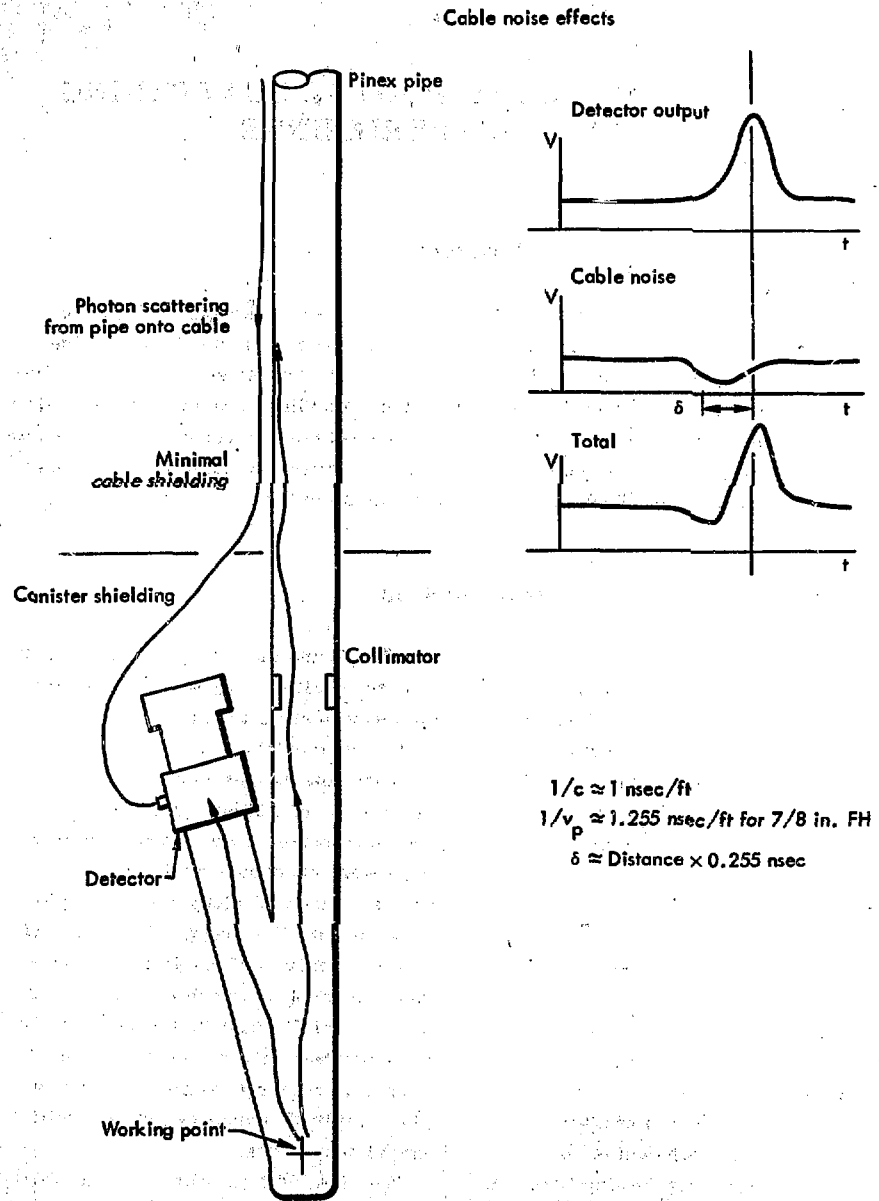

Fig. 1. Noise production on signal cables from pipe scattering.

means of calculating the amount of induced cable current is summarized in the Predicted Cable Noise Currents section, page 24.

Fluence Rate Calculations, Uncollimated Case

EXTERIOR PIPE REGION

Two calculational methods (hand and Monte Carlo) were used to predict the gamma energy fluence rate outside the pinex pipe. The hand calculation method used simplifying assumptions and neglected multiple scattering in the backfill material to calculate an "effective" volume of pipe from which the Compton scattered photons were emitted. These scattered photons were transmitted through the backfill and a solid angle factor was estimated to account for the photons that escaped.

The terms used to express the fluences are defined as:

$$\psi_s = \frac{\gamma \text{ MeV}}{\text{cm}^2 \text{ sec}} \text{ per } \frac{\text{source } \gamma}{\text{sec}} ,$$

which is the gamma energy fluence rate per source photon per sec, and

$$\dot{\phi}_s = \frac{\gamma}{\text{cm}^2 \text{ sec}} \text{ per } \frac{\text{source } \gamma}{\text{sec}} ,$$

which is the gamma fluence rate per source photon per sec.
The results of the hand calculation give:

$$\psi_s = 8.8 \times 10^{-12} \left(\frac{\gamma\text{-MeV}}{\text{cm}^2 \text{ sec}} \right) \Big/ \left(\frac{\text{source } \gamma}{\text{sec}} \right)$$

at a distance of 75 ft from the source and 1 in. outside the pipe.

In view of the approximations needed to arrive at the above calculation, a series of Monte Carlo calculations, taking into account detailed geometry and multiple scattering effects, were performed.

The photon fluence rate as a function of distance from the device was calculated using the SORS-G Monte Carlo photon transport code.[1] The SORS-G geometry for the non-collimated pinex line-of-sight (LOS) was approximated as shown in Fig. 2. Line-of-sight materials were 2 in. of Pb and 1/2 in. of SiO_2 located 13 ft from the source. A disk source was used with all photons aimed within a 19 in. diam disk located 35 ft above the source. The source energy spectrum was a Maienschein[2] fission spectrum. A low density counting region was placed around the pipe in an annulus 1 in. from the pipe o.d. The calculated energy spectrum of scattered photons (in zone 63 between 70 and 80 ft from the source) is shown in Fig. 3. The value of ψ_s as a function of distance from the source normalized to an experimentally measured point at 76.2 ft shows two peaks as seen in Fig. 4. The first peak is located approximately 60 ft from the source because of the effect of collimation within the diagnostic canister. The second peak is located near the pinhole region and is due to scattering from the front of the pinhole assembly.

The data point used in normalizing the SORS-G results shown in Fig. 4 was obtained by locating two detectors 1 in. outside the pinex pipe at 76.2 ft from the source.[3] A photograph showing the installation of one of these detectors is shown in Fig. 5. Within experimental error,

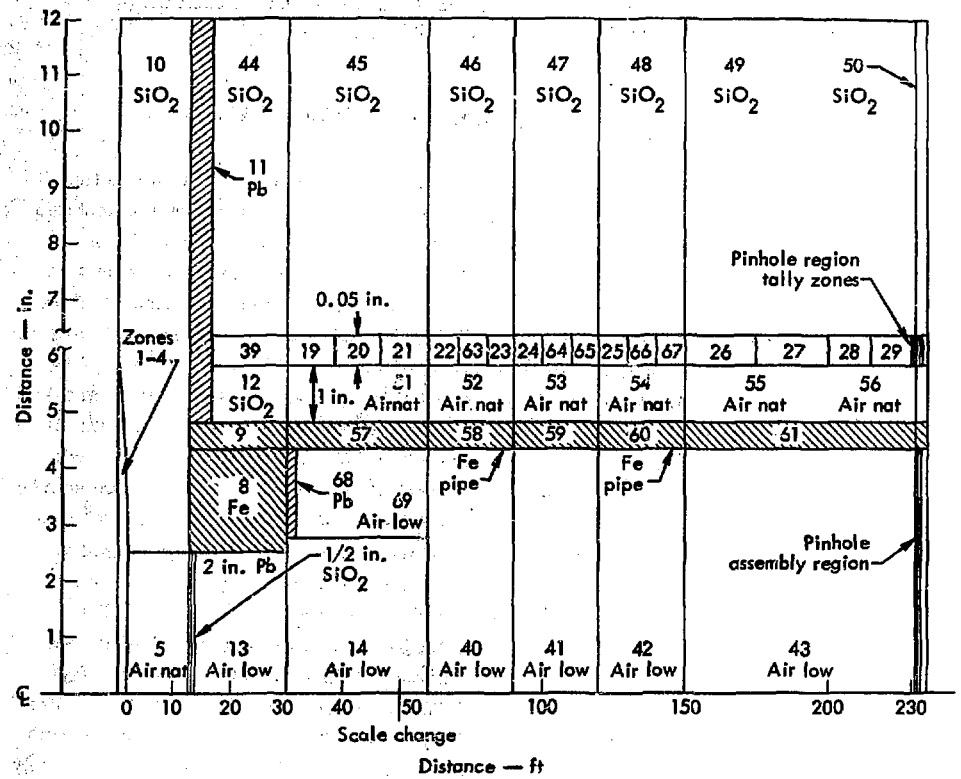

Fig. 2. Pinex pipe SORS-G geometry.

the measured data agreed with the unnormalized SORS-G results within a factor of 4. See Ref. 3 for detailed explanation of this experiment. For a cable sensitivity of 1.1×10^{-20} (A/m)/(γ MeV/cm^2 sec),[4] the measured fluence rate would induce $3.3 \times 10^{-32} \frac{\text{A/m}}{\text{source photon/sec}}$ at 60 ft in an unprotected cable 1 in. from the pipe.

PINHOLE ASSEMBLY REGION

The second peak shown in Fig. 4 at 230 ft required coarse zoning to avoid high statistical errors in the pinhole region. This did not allow adequate prediction of the energy fluence rate in that area outside the pipe. To study this region in greater detail, a second SORS-G problem was run using a disk source aimed directly at the pinhole assembly. The geometry for this problem is shown in Fig. 6. Results from this problem, using a steel pinhole assembly, indicate ψ_s peaks approximately 3 in. above the front face as shown in Fig. 7. The same problem run with a Pb pinhole assembly reduces ψ_s by approximately a factor of 2. Therefore, a 2 in. Pb front face for the pinhole

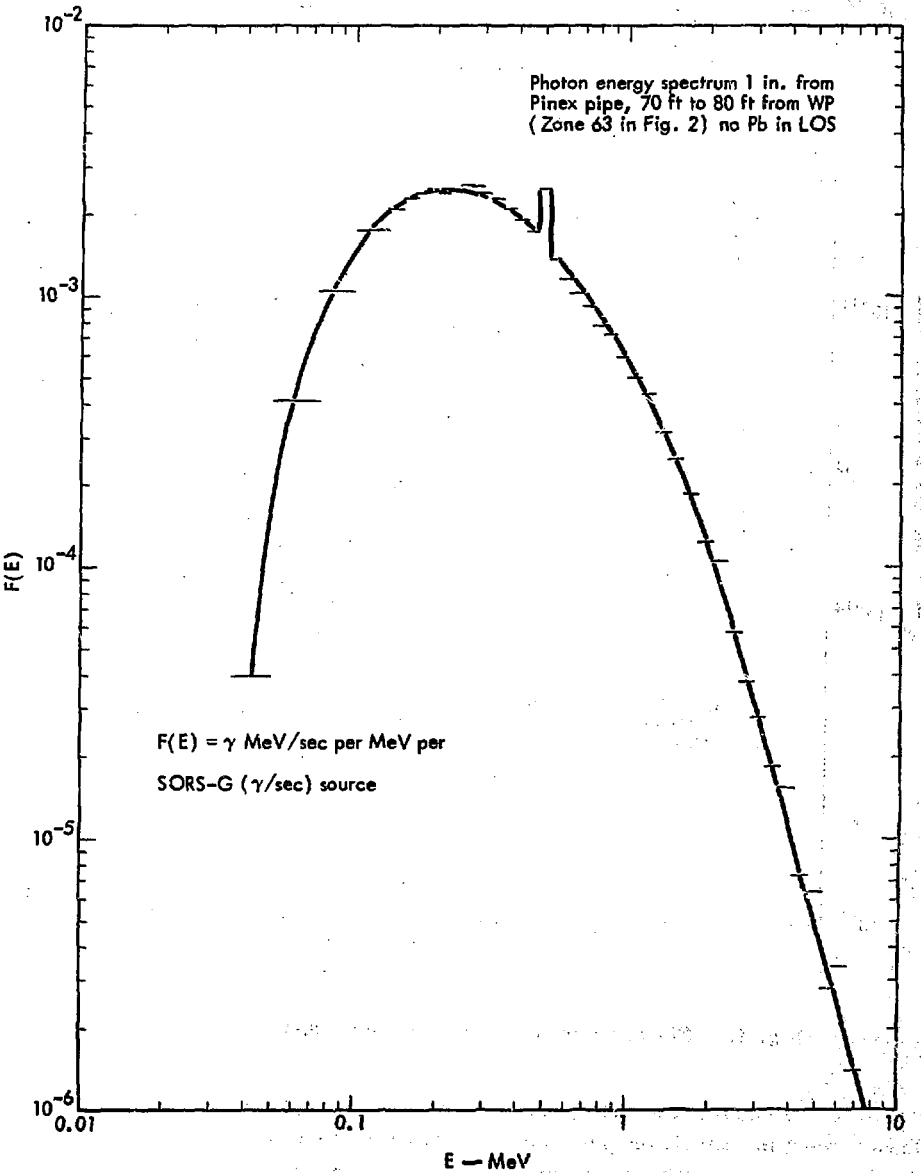

Fig. 3. Energy spectrum outside pinex pipe.

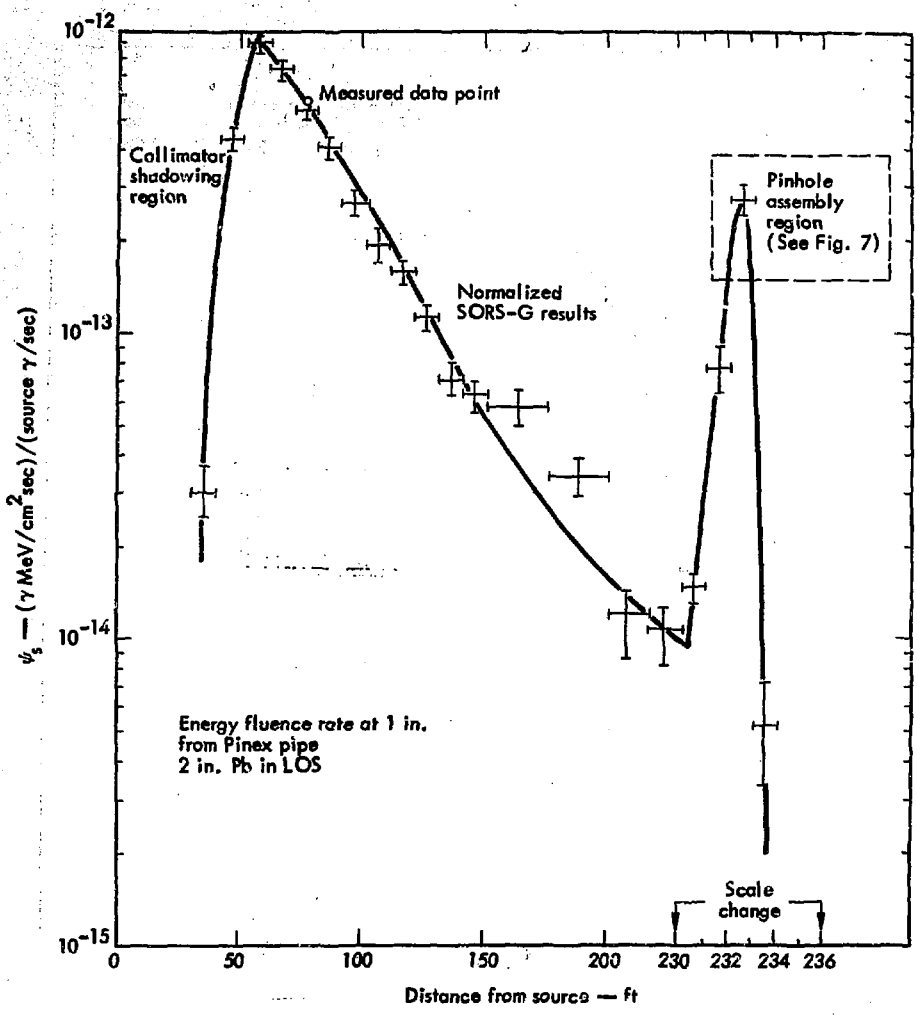

Fig. 4. Fluence rate vs distance from SORS-G calculations.

assembly is recommended. The peak fluence rate 1 in. outside the pipe in the pinhole region is somewhat higher for a short distance than the peak rate calculated at 60 ft in the previous problem. It is recommended that cable shielding in the pinhole region should be done with standard trays using a Pb front face on the pinhole assembly. The amount of shielding depends on time dependent effects and the signal-to-noise ratio required.

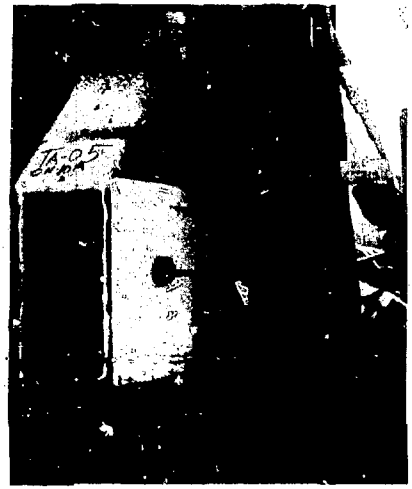

Fig. 5. Photograph of detector installation.

CABLE TRAY REGION

The standard cable tray design, shown in Fig. 8, uses a 6 in. steel channel stood off 6 in. from the pipe. The standoff distance and tray width was chosen originally to eliminate a direct path from the pipe to the trays. Each tray section is 5 ft long and can be fitted with Pb sides and cover. In order to optimize the tray design, the effect of standoff distance and effect of tray sides and cover was studied. To understand these effects, the geometry of Fig. 8 was zoned in another SORS-G problem as shown in Fig. 9. The inside pipe wall was the source with all photons incident at less than 1° angle from the pipe centerline. Sand (SiO_2 of density

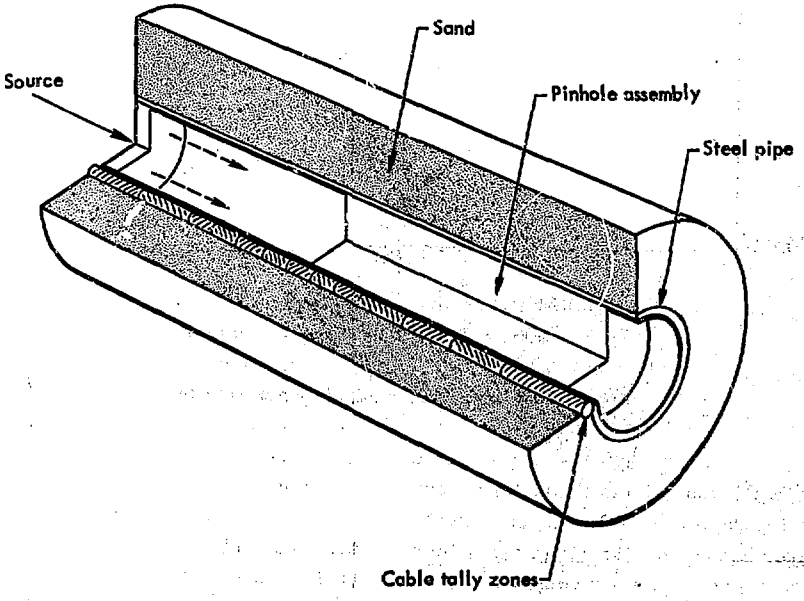

Fig. 6. SORS-G pinhole geometry.

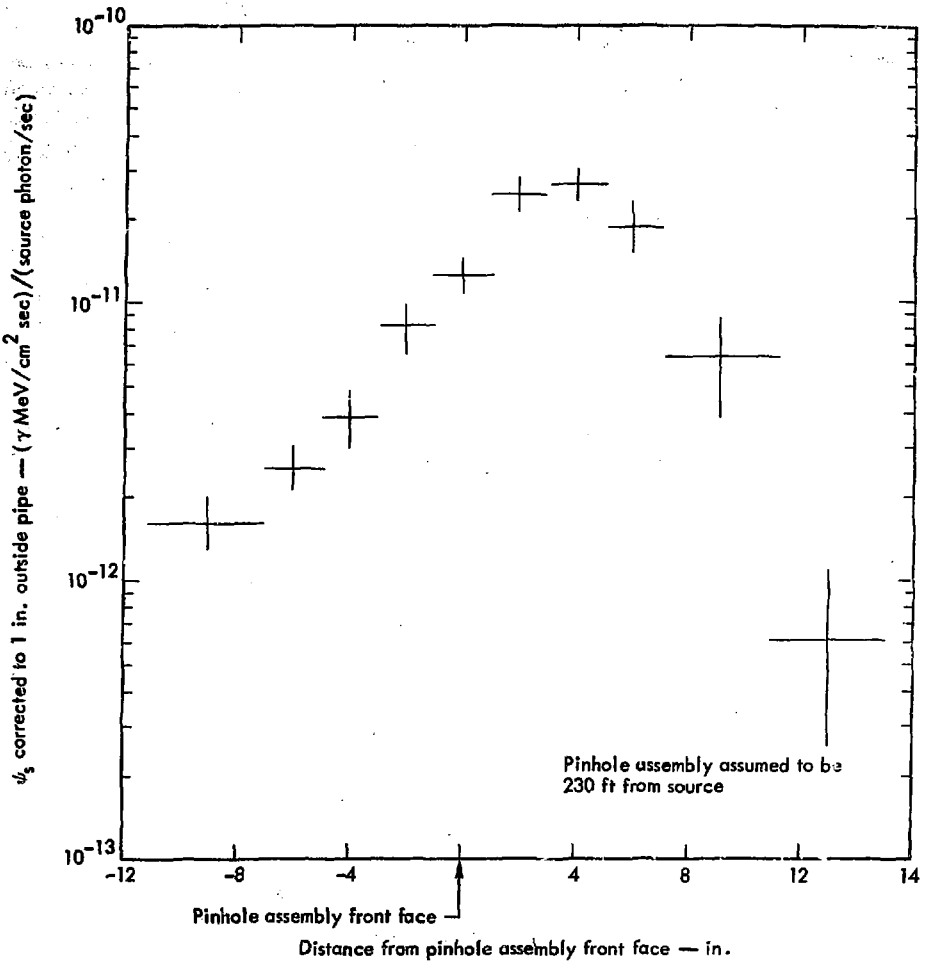

Fig. 7. Results from SORS-G pinhole region.

1.5 g/cm^3) was used as the material surrounding the pipe and trays. The effect of sides and cover for various tray thicknesses was evaluated by comparing a number of SORS-G problems. End effects from the zoning were minimized by evaluating only the center zone of the trays.

Table 1 lists the relative energy in the trays for various configurations of tray thickness, sides and covers in the standard design stood off 6 in. from the pipe. The SORS-G results were normalized to the case with 1 in. of Pb tray thickness, 1/4 in. Pb sides, and a 1/4 in. Pb cover.

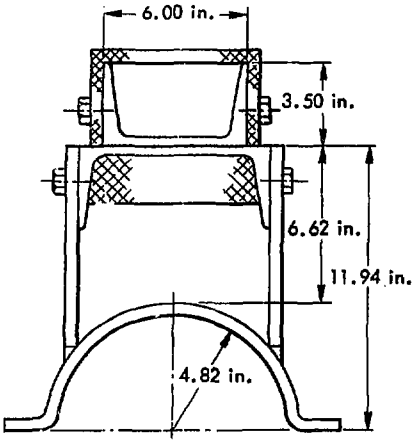

Fig. 8. Standard cable tray.

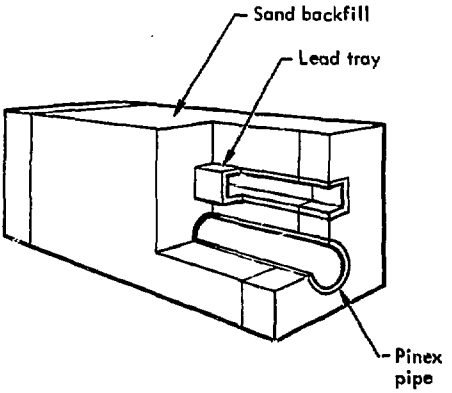

Fig. 9. SORS-G cable tray geometry.

Table 1. Cable tray design parameters (6 in. standoff).

Pb sides and Pb cover	Front tray thickness		
	1 in. Pb front	2 in. Pb front	3 in. Pb front
No sides, no cover	3.16 (388)[a]	2.1 (219)	Not calculated
1/4 in. sides, no cover	1.17 (695)	0.28 (560)	Not calculated
1/2 in. sides, no cover	1.05[b] (674)	0.22 (658)	Not calculated
1/4 in. sides, 1/4 in. cover	1.00[bc] (798)	0.15 (751)	0.04 (770)
1/2 in. sides, 1/2 in. cover	0.94 (818)	0.10[b] (796)	0.01[b] (600)

[a]The number in parentheses indicates the average energy in keV.

[b]Recommended configuration.

[c]Normalized to 1.0 at 1 in. Pb front, 1/4 in. Pb sides, 1/4 in. Pb cover, 6 in. wide tray, 9-5/8 in. o.d. pipe. Tray inside 6 in. from pipe outside.

The average energy in the tray obtained from the SORS-G calculation is listed for estimating cable sensitivity corrections. Tray sides are recommended for all cases because of multiple scattering in the stemming material. Tray covers are recommended when at least 2 in. of Pb tray thickness is required. The requirements for tray thickness are dictated by the source strength and signal-to-noise ratio that can be tolerated in a particular experiment.

The effect of the standoff distance from the pipe was calculated for two arrangements of Pb shielding. The results of these calculations showing the relative energy in the tray as a function of standoff distance are shown in Fig. 10. Also

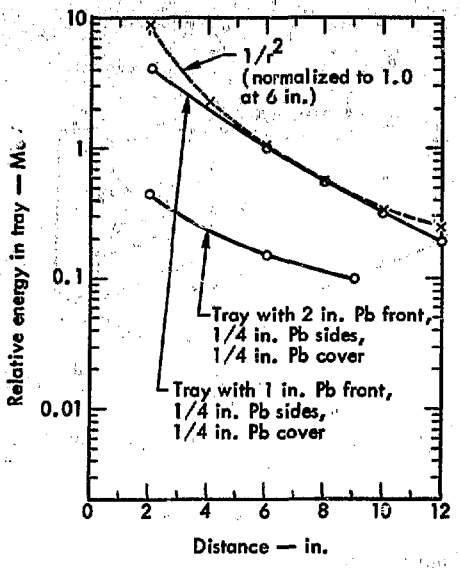

shown is a $1/r^2$ curve normalized at 1.0 at 6 in. standoff distance. Figure 10 indicates the tradeoff between Pb thickness and standoff distance. In addition, increased standoff distance helps eliminate direct shine.

Fig. 10. F ergy inside the cable tray vs standoff distance.

Fluence Rate Calculations, Collimated Case

The previous section (pages 3 through 10) described the case when the pinex pipe inner wall is exposed to photons along most of its length with collimators located only in the diagnostic canister section. A second case, using collimators inside the pipe wall, localizes the scattering at the collimators and does not allow the photons to impinge along the entire LOS pipe. The signal cables are protected near the collimators and stood off from the pipe but do not require a continuously shielded cable run along the full length of the pipe. From this standpoint the collimated system is more economical since it reduces the quantity of lead required. However, a vacuum system is required (or additional Pb protection) to avoid noise induced by air scattered photons (see page 14).

In a collimated LOS, considerations such as source diameter at maximum gamma output, collimator aperture, LOS pipe diameter, and collimator tolerances determine the number and location of the collimators. The standard collimated case uses 13-3/8 in. pipe (as opposed to 9-5/8 in. o.d. pipe in the uncollimated case) with 1 ft long, 6 in. aperture Pb collimators. The purpose for using large diameter pipe is to minimize the number of collimators and shielding required.

COLLIMATOR REGION

To design adequate cable protection near the collimators, the energy and angular distribution of the photons emerging from the pipe and scattering back from the stemming material was calculated using the SORS-G Monte Carlo code.

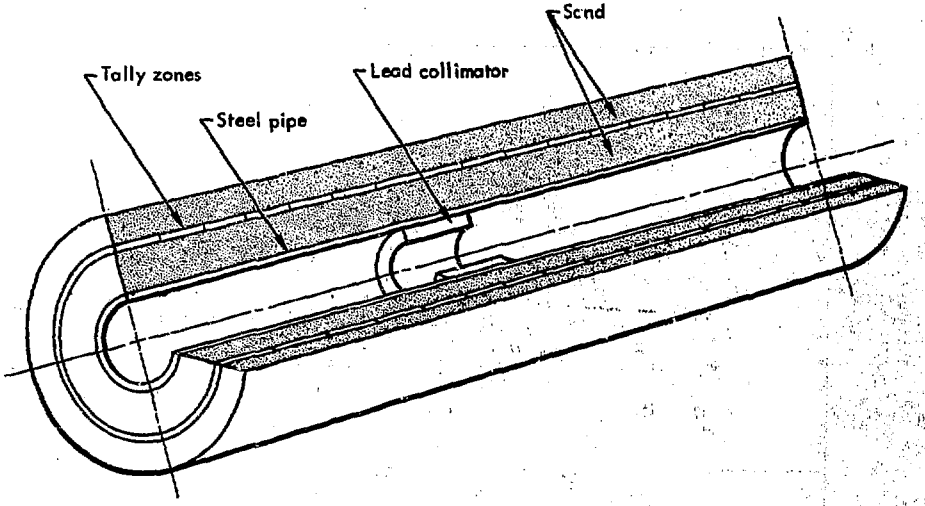

Fig. 11. SORS-G collimator geometry.

The geometry, shown in Fig. 11, used zoning which included a thin, very low density, tally zone placed at various distances from the pipe.

The material exterior of the pipe was SiO_2 at a density of 1.5 g/cm^3. This simulates Overton sand which is the standard stem. ing material used for pinex experiments. The normal density of Overton sand is about 1.75 g/cm^3, but since it has a tendency to "bulk" during the stemming process, the lower density value was used.

The source annulus had an inner diameter equal to the collimator aperture and an outer diameter 1 in. less than the pipe i.d. The size of the annular i.d. was chosen to reduce statistical variation; i.e., not allow the photons to leave the source and immediately exit the problem from the top of the LOS. The size of the annular o.d. was chosen because of previous field criteria; that is, it allows slight bowing of the pipe and still prevents photons from impinging directly on the LOS pipe. The energy spectrum from the source was a fission spectrum which had been hardened by transmission through exterior materials (the standard neutron pinex and device canister materials).

Figure 12 shows the fluence rate, ϕ_s, exterior to the LOS pipe as a function of distance from a 6 in. aperture collimator. The two histograms represent scattering into zones immediately exterior and 10 in. from the pipe.

The greatest fluence rate occurs below the collimator and is caused mainly by back-scattered photons. The fluence rate is low in the region immediately above the collimator, but increases and peaks about a foot above the collimator. This peak can be explained by Fig. 13. Photons entering the collimator near the aperture

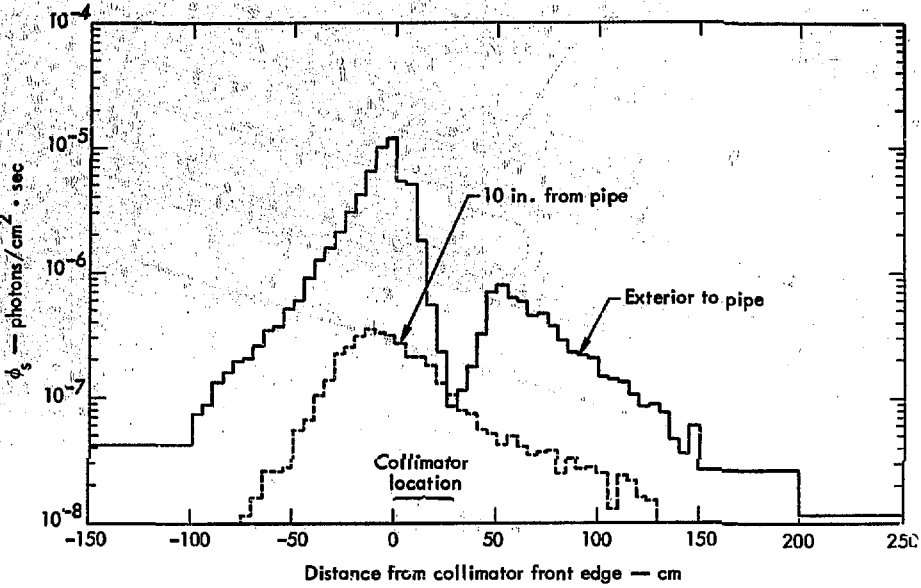

Fig. 12. Photon fluence rate vs distance from collimator.

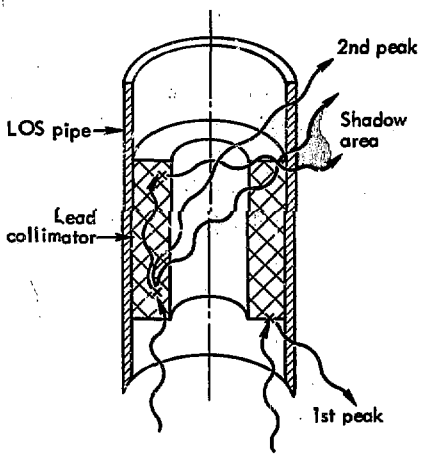

Fig. 13. Illustration of collimator scattering.

may scatter at low angles through the aperture and impinge on the pipe wall above the collimator. The "shadow area" between the collimator and the second peak develops because the photons must penetrate more lead to arrive in that area; i.e., the photons can penetrate deeper into the collimator and then scatter behind the opposite edge of the collimator, or penetrate a short distance into the collimator, scatter through the aperture and penetrate the back part of the opposite side of the collimator to reach the "shadow area." Whatever route the photons travel involves a deep penetration of a high Z material, and consequently a large loss of intensity.

The effect of increasing aperture size, shown in Fig. 14, causes a corresponding increase in ϕ_s at the second peak. This is consistent with the previously discussed

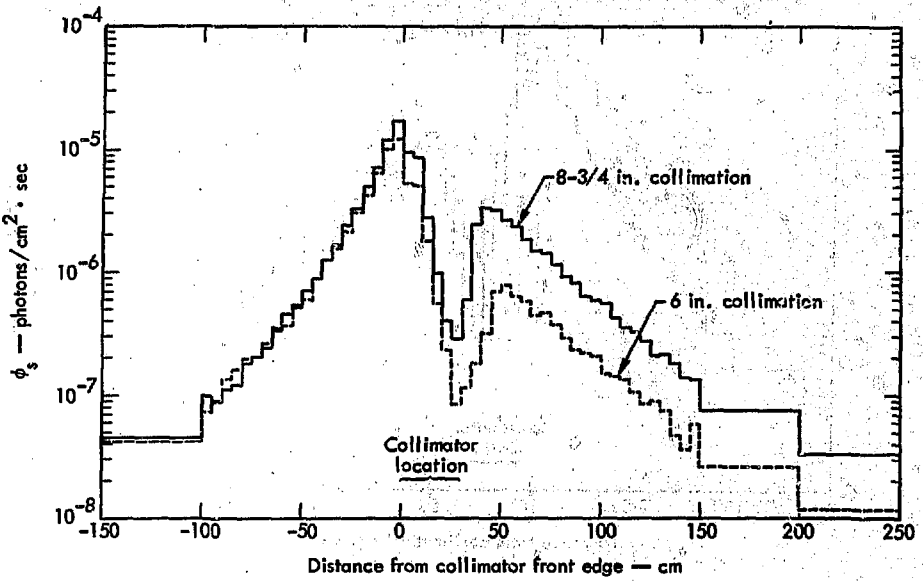

Fig. 14. Effect of increasing aperture size for the collimated case.

cause of the second peak and is a further reason to collimate with small apertures.

Figure 15 compares the photon and photon energy fluence rates, ϕ_s and ψ_s, as a function of distance from the collimator for the case of a 6 in. aperture. There is a definite change in the average energy per photon along the LOS pipe with respect to the collimator location, beginning with the relatively soft spectrum below the collimator to a harder spectrum above the collimator. Figure 16 shows the energy spectrum of the photons emerging from the LOS pipe at 0 to 5 cm (zone 22) below the collimator and at 40 to 45 cm (zone 33) above the collimator (the approximate location of the peaks in Fig. 12). The higher energy photons enter the tally zone from the LOS pipe at an angle dependent upon location from the collimator but the photons between 100 and 200 keV enter the zone from the stemming material and the pipe. The photons below 100 keV come primarily from the stemming material because the sand has a very low photoelectric absorption cross section. Thus, a photon may scatter many times in the sand before being absorbed (averaging about 20 scatters). Photons of 50 keV have an equal probability of being absorbed or rescattered.

In the region below the collimator, the energy spectrum is soft because of back scattering. For instance, a Compton scattered 3 MeV photon is reduced to between 440 and 230 keV for scattering angles between 90° and 180°, respectively. However, as illustrated in Fig. 16, the

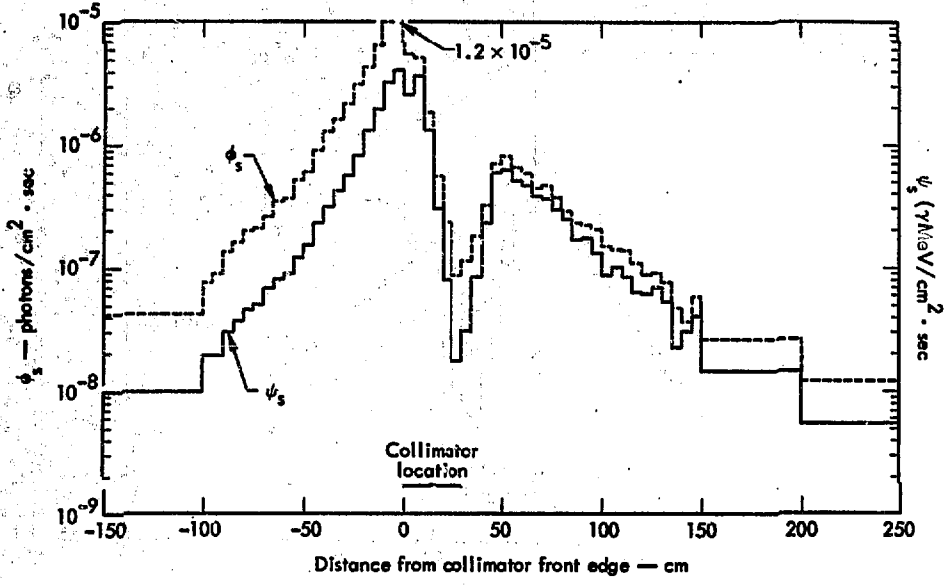

Fig. 15. Photon and energy fluence rate vs distance from the collimator.

dominant energy tally group (466 keV to 513 keV) is caused from the annihilation radiation (511 keV) of the positrons generated during pair production. Also, Fig. 16 shows the energy spectrum for the tally zone (above the collimator) where ϕ_s has a second peak. The energy spectrum is fairly smooth in this region of the LOS pipe, but the angle of incidence is peaked around 60° for most energies (except below 200 keV). In addition, as the distance above the collimator is increased, the angle of incidence also increases.

AIR SCATTERING CONTRIBUTIONS

Diagnostic systems requiring a long LOS pipe frequently utilize an evacuated LOS. However, if the LOS is not evacuated, or if the vacuum system fails, the air can cause sufficient scattering to induce noise currents in nearby cables. A series of SORS-G calculations were done in which this type of scattering was studied.

Problems were run to simulate various cable standoff distances from the LOS pipe. The geometry was again a 13-3/8 in. pipe surrounded by sand (SiO_2, ρ = 1.5 g/cc) with very thin, very low density tally zones located exterior to the pipe, 6 in. and 10 in. away. With the LOS at atmospheric pressure (ρ = 0.00129 g/cm^3), the resultant fluence rates in the tally zones were:

Standoff distance (in.)	$\left(\frac{\gamma/cm^2\ sec}{source\ \gamma/sec}\right)$
0	4.7×10^{-7} (0.5 MeV)
6	9.9×10^{-8} (0.3 MeV)
10	3.4×10^{-8} (0.3 MeV)

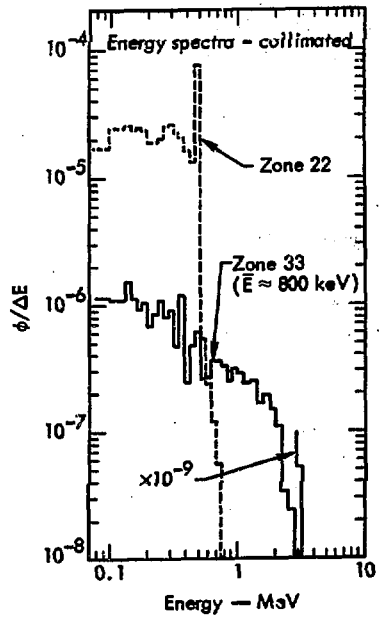

Fig. 16. Energy spectrum of scattered photons from collimator.

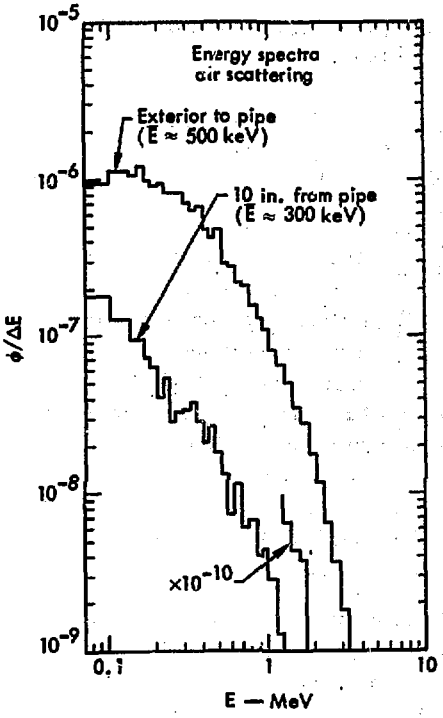

Fig. 17. Energy spectrum of scattered photons from air scattering.

The above numbers do not include any source solid angle corrections. The solid angle correction required is $A/4\pi R^2$ where $A = 652$ cm^2 and R is the distance from the source to the required location in centimeters. Thus, by placing the cables greater than 10 in. away from the LOS pipe, a reduction in the fluence rate greater than a factor of 10 can be achieved. Also, any reduction in the LOS pressure below atmospheric also reduces ϕ_s, since the density is directly proportional to the linear attenuation coefficient (μ). The average photon energy in the region adjacent to the LOS pipe is approximately 500 keV (see Fig. 17), which is less than the average energy of photons in the same region above a collimator (approximately 800 keV).

CABLE TRAY DESIGN— COLLIMATOR REGION

Excessive machine time would be required using the SORS-G code to obtain adequate statistics inside the cable trays. Therefore to design adequate Pb tray shielding near a collimator, a deep penetration Monte Carlo transport code, possibly using the statistical estimation technique, would be required.[5] However, this problem was approached in a different manner. The SORS-G code was used to establish the fluence rate on the trays, then the photons in each energy group

were transported through the Pb tray by the following means:

$$\phi_s = \sum_{i=1}^{n} \phi_i' b_i e^{-\mu_i x} \qquad (1)$$

where

ϕ_s = fluence rate inside the tray per source photon per sec

ϕ_i' = fluence rate outside the tray per source photon per sec per energy group (SORS-G output)

b_i = buildup factor per energy group

μ_i = linear attenuation coefficient per energy group

x = tray thickness

n = number of energy groups (usually 50)

A more exact form for calculating ϕ_s, including angular distribution contributions, is contained in Appendix B. The SORS-G code had been used to obtain the angular distribution, but this data proved unreliable due to poor statistics. Because of this, the photons were assumed normally incident to the tray. This assumption produced an overestimation of ϕ_s which in turn required more Pb in the trays and thus a more conservative shielding criteria. The buildup factors were estimated using the same assumption; i.e., the buildup factors were taken assuming a plane monodirectional source.[6] Though ϕ_s can be fairly accurately calculated using buildup factors, a value of ψ_s obtained by multiplying ϕ_s by $\bar{E}$ would be overestimated. This overestimation occurs because many of the photons contained in the buildup factor are below the lower energy limit of the energy group being summed.

Table 2 contains the results of the above calculation for the zone above and below the collimator in which the greatest energy fluence rate, ψ_s, was incident. A 4 in.

Table 2. Fluence rate inside cable trays, $\phi_s \left(\frac{\text{photons/cm}^2 \text{ sec}}{\text{source photon/sec}}\right)$[a]

Tray location	2 in. Pb tray[b]	4 in. Pb tray[c]
0 in.	7.6×10^{-10} (0.9)[d]	3.3×10^{-9} (2.0)
6 in.	1.1×10^{-11} (0.5)	1.5×10^{-10} (1.8)
10 in.	3.4×10^{-12} (0.5)	4.5×10^{-11} (0.9)
	Air scattering (STP air in pipe)	
0 in.	7.6×10^{-9}	
6 in.	5.1×10^{-10}	
10 in.	1.0×10^{-10}	

[a]The ϕ_s shown were calculated in the zones at which the energy fluence rates are the greatest. Geometry was for 13-3/8 in. pipe and 6 in. aperture collimator.

[b]Recommended configuration includes 1/2 in. Pb sides and 1/2 Pb cover.

[c]Recommended configuration includes 1 in. Pb sides and 1/2 in. Pb cover.

[d]The number in parentheses indicates the average energy in MeV of ϕ_s.

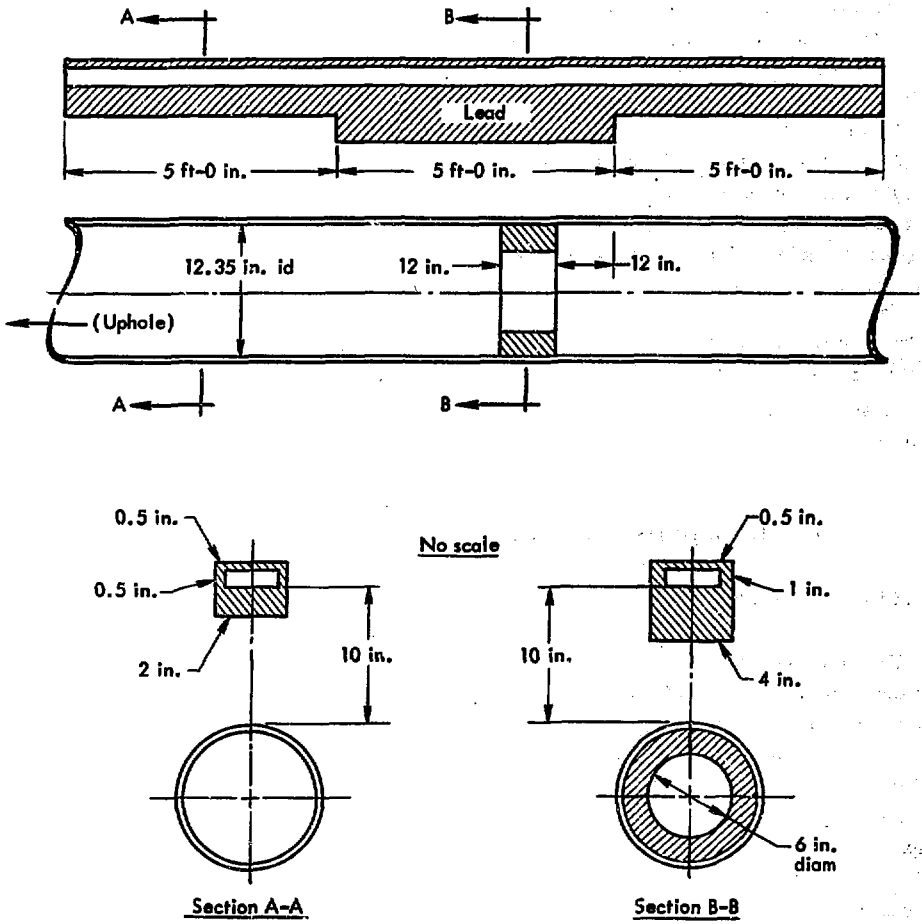

Fig. 18. Shielding for collimator region.

lead tray was used above the collimator in the region of peak ψ_g, while a 2 in. tray was used below. (Figure 15 indicates the fluence rates directly outside the pipe, and shielding for this case was based on this result.) The distance the shielding extends above and below the collimator can also be approximately determined from the SORS-G results. The requirement for shielding was discontinued when ϕ_s decreased to approximately 10^{-10} photons/cm^2 sec per source photon per sec (10 in. away from the LOS pipe). The SORS-G statistics were bad in these regions, so the tray lengths are approximations.

The recommended side thicknesses are 1 in. of Pb for the 4 in. tray and 1/2 in. of Pb for the 2 in. tray. The

covers in both cases should be 1/2 in. of Pb. The contribution of photons entering the cable area through the sides and cover is small and does not contribute significantly to the fluence rates shown in Table 2. Also, for manufacturing and fielding ease, no change in the tray thickness as a function of distance from the source is made. These recommendations are shown in Fig. 18.

CABLE TRAY DESIGN— AIR SCATTERING EFFECTS

As stated previously, even though the cables are stood-off, air scattering in the LOS can contribute significantly to an induced current in the cable. Thus, if the LOS is not evacuated, the cables should be shielded. Using the same calculational method as in Eq. (1) and a Pb thickness of 2 in. at the given standoff distances the resulting fluence rate, ϕ_s, is as shown in Table 2 (Air Scattering). The average photon energy in the tray at the three distances is about 2 MeV per photon. Thus, if the trays are 2 in. thick, they should be stood-off at least 10 in. Again, the sides and cover thicknesses are the same as those given in the uncollimated case for the respective tray thickness.

Cable Sensitivities and Time Dependent Effects

CABLE SENSITIVITIES

Probably one of the larger uncertainties in determining the magnitude of induced current in a cable is that of the cable sensitivity to incident photons. The purpose of this section is simply to present compiled information from various sources that may be of value to experimenters. Table 3 contains a tabulation of the results from three separate sources.

The third tabulation is the result of a comparison study prior to the Arnica Event.[7] A high velocity cable was desired to reduce the signal-to-noise ratio but not at the expense of increased sensitivity. Part of this study was made using the Pulsed Febitron to simulate the event environment, but because of the low sensitivities involved, the source needed to be close to the experiment resulting in poor geometry. Though the relative sensitivities were established, the accuracy of the measured values is questionable.

Many parameters affect a given cable's sensitivity and these need further investigation. The areas include sensitivity versus incident photon energies, sensitivity versus cable bias voltage (such as an electrical signal propagating in the cable at the time of irradiation), cable dielectric ionization effects, nanosecond transient effects from a pulsed source, etc. Williams and Mead[8] reported on the effects of dielectric ionization several years ago. Also, G. Allen (EG&G) demonstrated significant changes in cable sensitivity by varying the bias voltage on several cable types. Results of his study are shown in Fig. 19. Additional studies are planned to establish energy versus sensitivity curves for various cable types. One such study will include measurements using lower energy monoenergetic sources

Table 3. Cable sensitivities to gamma radiation.

Cable type	Measured sensitivities[a]	
C. Williams and J. Mead[8]		
	^{60}Co	$\bar{E}$ = 3.2 MeV
7/8 in. Foamflex	-1.5	-0.46
7/8 in. Styroflex	-1.5	
RG 58	-0.2	
RG 8	-0.16	
D. L. Redhead[4]		
	^{60}Co	2 MeV Pulsed Febitron[b]
7/8 in. Foamflex	-1.1	-2.10 V
1/2 in. Foamflex	-0.52	-2.25 V
RG 219	-0.77	-1.12 V
T. Rottunda[7]		
	^{60}Co	100 keV dc x-ray / 2 MeV Pulsed Febitron
7/8 in. Foam Heliax	-0.69	-9.5 / -0.14
7/8 in. NHJ-5 (low density foam)	-0.18	0[c] / -0.43
7/8 in. Air Heliax	-140.00	-7900.0 / -0.21
1-5/8 in. Air Heliax	-110.00	-4600.0 / (not attempted)

[a] $10^{-20} \frac{A/m}{\gamma\text{-MeV/cm}^2 \text{ sec}}$, cables unbiased.

[b] Relative comparison (volts).

[c] No significant current above background.

and also a Monte Carlo photon-electron transport code. However, this investigation has just begun and it will be some time before the results are obtained.

TIME DEPENDENT EFFECTS

Photon induced noise on cables occurs when the gamma intensity from the reaction peak catches up with slower electrical signals in cables and induces current in the cable comparable to the signal current (Fig. 1). Thus shielding considerations should be based on signal-to-noise ratio and the amount of shielding required is a function of the shape of the signal, the cable velocity, and the maximum acceptable noise current at each position along the pipe. A fast cable such as Andrews NHJ-5 has a higher signal-to-noise ratio near the device due to higher signal currents at high fluence locations, thus moving the problem area farther from the source, allowing the $1/R^2$ effect to reduce the fluence rate. An example of the effect of faster cables on the ratio of signal-to-pipe fluence rate is shown in Fig. 20. A

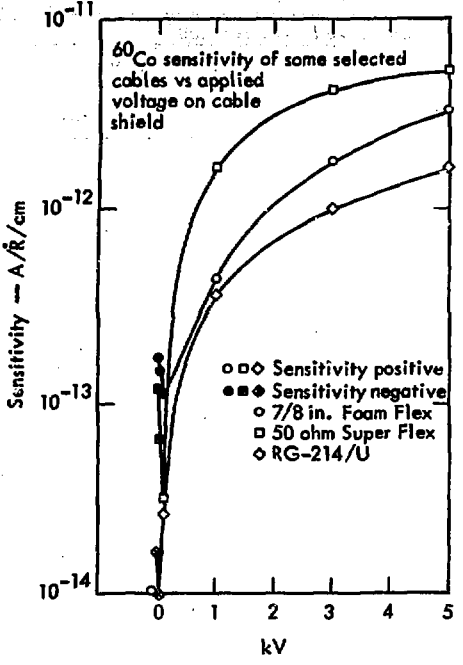

Fig. 19. Cable sensitivity vs bias voltage.

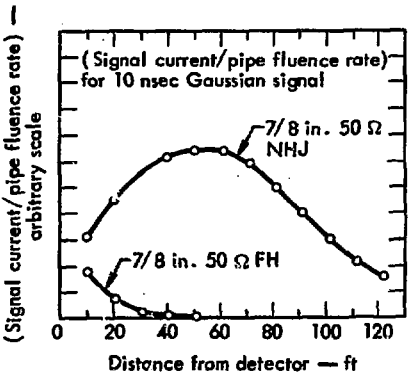

Fig. 20. Relative signal-to-noise ratio vs feet from detector.

10 nsec gaussian pulse was assumed to be incident on a detector, with the fluence rate in the pipe falling off as $1/R^2$. Since the fluence rate in the pipe is related to noise induced in the cable, the ratio of (signal current/pipe fluence rate) as a function of distance from the device is related to the shielding required. Figure 21 shows how the NHJ-5 cable moves the interaction between earlier detector signals in the cable and the peak gamma induced signal farther from the detector than the standard 7/8 in. FH cable.

However, there is an adverse effect from using high velocity cable if the cable runs are parallel to the LOS for long distances. The difference between the photon velocity and the propagation velocity of the cable can cause a buildup of the radiation induced current. Thus, for each foot

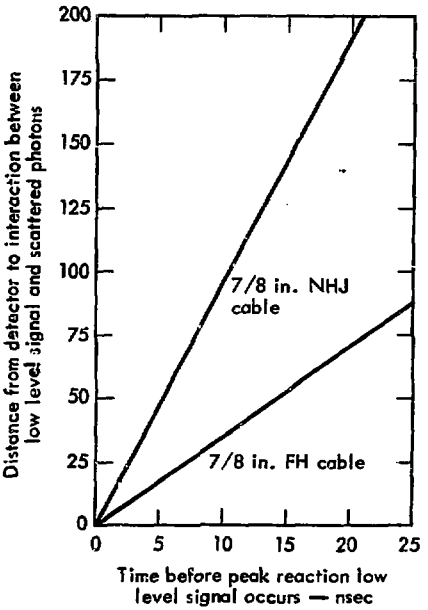

Fig. 21. Distance from detector for peak noise to hit cable vs time before peak low level signal occurs for 7/8 in. FH cables.

Given a source intensity, $S(\lambda)$, plotted as a function of time (right), it can also be plotted as a function of distance (below).

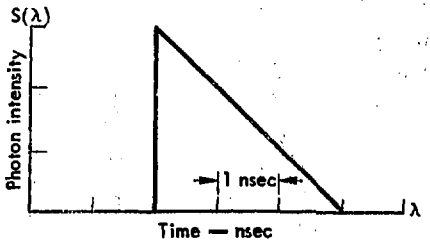

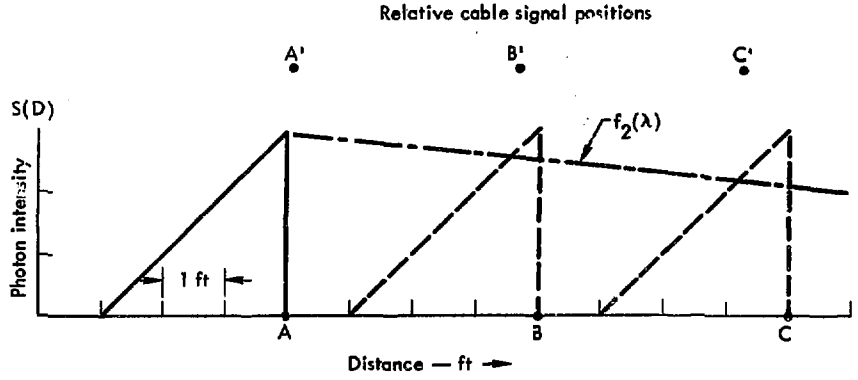

Assume v_γ = 1 nsec/ft and v_c = 0.9 nsec/ft, then positions A, B, and C represent $S(\lambda)$ vs distance at some relative time, λ = 0, 4, and 8 nsec. Positions A', B', and C' represent *the location of the A' electrical signal in the cable at these respective times. Then,* $f_2(\lambda)$ describes the photon intensity with respect to this electrical signal.

Fig. 22. Graphical illustration of current buildup.

traveled, the electrical signal induced in the previous segment is only a fraction of a nanosecond behind the photons that had induced the current. Since the source intensity, $S(\lambda)$, is a function of time, additional current will be induced upon the existing current propagating in the cable. (λ is a dummy variable for time.)

Given such a source intensity distributed in time it can also be plotted as a function of distance along the LOS (Fig. 22); i.e., $d = v_\gamma \lambda$ where d = distance in ft, v_γ = photon velocity (~ 1 ft/nsec), and λ = time in nsec. In this illustration, it is assumed that the cable propagation velocity v_c is 0.9 ft/nsec. At point "A,"

a signal is induced in the cable by the peak intensity. One nsec later, the photons have traveled 1 ft while the signal has only traveled 0.9 ft. Now a signal is induced on the existing signal in the cable by a source intensity dependent upon the cable velocity. As λ is increased each $\Delta\lambda$ the phenomenon is repeated. Thus, a new function describing the source intensity (as seen by an electrical signal in the cable) is established:

$$f_2(\lambda) = S[(1 - v_c/v_\gamma)\lambda]. \quad (2)$$

However, several important considerations have been neglected; i.e., the solid angle effect and the photon transmission. Thus, a general equation describing the current buildup can be written as follows:

$$I_c(t) = \frac{K}{4\pi}\int_{-\infty}^{\infty} \times \frac{e^{-\mu[v_c\lambda - v_\gamma t]}\, S[t + (1 - v_c/v_\gamma)\lambda]}{[v_c\lambda - v_\gamma t]^2}\, d\lambda \quad (3)$$

or

$$I_c(t) = K\int f_1(\lambda)\, f_2(t + \lambda)\, d\lambda \quad (4)$$

where:

$I_c(t)$ = current induced in the cable (amps)

K = conversion factor between photon fluence rate in LOS and current in the cable (I_c)

$$f_1(\lambda) = \begin{cases} 0, \lambda < r_{min}/v_\gamma \\ \dfrac{e^{-\mu r}}{4\pi r^2}, \dfrac{r_{min}}{v_\gamma} \leq \lambda \leq \dfrac{r_{max}}{v_\gamma} \\ 0, \lambda > r_{max}/v_\gamma \end{cases}$$

$$f_2(\lambda) = S[(1 - v_c/v_\gamma)\lambda]$$

$$r = v_c\lambda - v_\gamma t$$

r_{min} = distance below which no current can be induced

r_{max} = distance above which no current can be induced

μ = linear attenuation coefficient.

To understand Eq. (4), refer to Fig. 23. For some t, $f_2(\lambda)$ lies between r_{min}/v_γ and r_{max}/v_γ and the equation integrates the product of the two functions (between a and b since the product is zero elsewhere). As t is increased (later times on the cable signal), $f_2(\lambda)$ scans the $f_1(\lambda)$ function with the integration taking place over λ at each t. Note that $f_2(\lambda)$ scans to the left with increasing t, since the photons travel faster than the electrical signal and thus later scattering (farther up the LOS) induces signals that arrive at the recording facility first. Also, t lies between $\pm\infty$, but $I_c(t)$ exists only when the two functions overlap in λ time with one another.

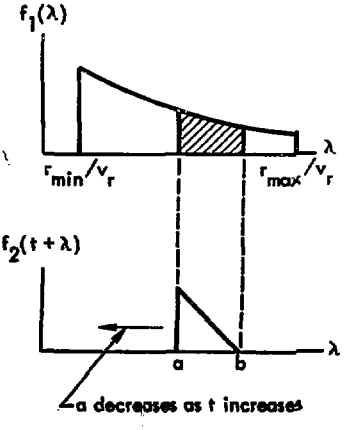

Fig. 23. Graphical illustration of the mathematical equation for I_c.

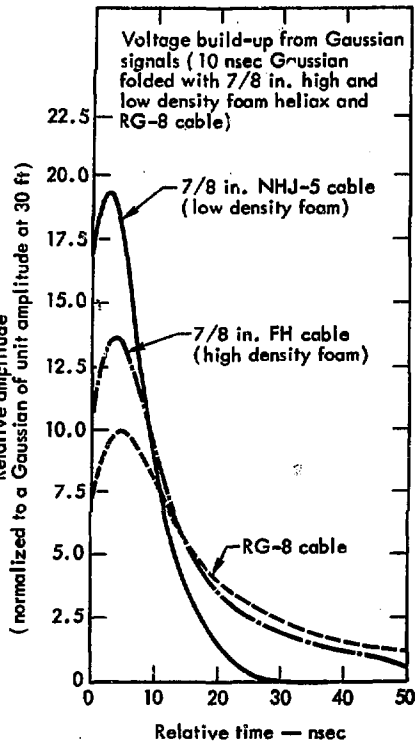

Fig. 24. Voltage buildup vs cable velocity.

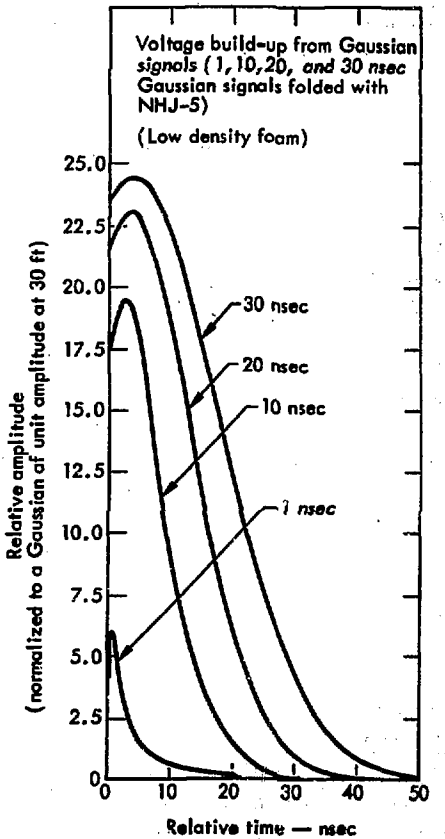

Fig. 25. Voltage buildup vs Gaussian width.

To obtain the magnitude of the problem, a code was written for the CDC 6400 (AEC-NVOO Centralized Computer System) which integrated these time and distance effects. Several assumptions were made in the code. First, the velocity of the photons was assumed to be 1 ft/nsec. Also, the linear attenuation coefficient used was for air at 0°C and 760 mm, and an average photon energy of 2 MeV. The current buildup induced by a 10 nsec wide (FWHM) gaussian signal on cables with different propagation velocities is shown in Fig. 24. Though the high velocity cables experience larger buildup, the curves decay rapidly to values below the lower velocity cables, thus providing better signal-to-noise ratios after the cross-over point. Figure 25 shows the buildup effect on NHJ-5 (7/8 in. low density foam) by varying the width of the gaussian source intensity. The curves for both figures were calculated assuming no scattering below 30 ft in the LOS (top of a standard π canister), or above 200 ft (assumed position of the pinhole assembly). The pinhole parameter not only has an effect on the

resultant buildup shape, but even on the maximum value if the pinhole is located close in for magnification purposes.

The code is now being modified so that a source intensity shape can be inputed with a "gamma per volt" detector value, and the detector location, then the resulting detector plus noise signal will be outputed with the correct time shift.

The effect the factors discussed in this section have on shielding criteria may differ greatly for each case because of the uniqueness of most experiments. The individual experimenter must sort through the various trade-offs available to optimize the success of the experiment. Some of these trade-offs are cable frequency response vs cable sensitivity, radiation environment vs cable sensitivity, and signal-to-noise relationships. Factors that affect the signal-to-noise ratio include pulse shape, cable propagation velocity, detector "roadmap" coverage, time dependent buildup factors, experimental geometry, etc. Thus, the experimenter must sort through these options to establish the final criteria. The recommendations contained in this report are for the more or less standard pinex experiments.

Predicted Cable Noise Currents

UNCOLLIMATED CASE

The photon transport calculation, described in the Fluence Rate Calculations, Collimated Case section, page 3, can be used in conjunction with measurements of the cable sensitivity described in the Cable Sensitivities and Time Dependent Effects section, page 18, to predict the induced cable current as a function of distance from the source and shielding parameters used. This calculation of induced current in a cable is intended to serve only as a guide due to the experimental error involved. The measured cable sensitivities, usually reported in units of A/m per γ MeV/cm^2 sec, are first converted into units that can be related directly to the SORS-G output. The desired units are: A/m/γ MeV/cm^3 sec (see Appendix A). The results of the conversion calculation give a sensitivity, S_γ, for 7/8 in. FH cable of 2.6×10^{-19} (A/m)/(γ-MeV/cm^3 sec).

The SORS-G code gives the energy deposited per cm^3 in the tray volume per photon striking 120 cm of pipe (length of counting zone). To estimate the energy actually deposited per cm^3 of cable, the SORS-G calculation was done with atomically mixed $Cu_{16}C_{28}H_{56}$ at 2.2 g/cm^3 in the tray to simulate cable density and material. Then, the relationship between the SORS-G problem which used the pipe wall as a source and the actual source can be calculated by a solid angle correction of $A/4\pi R^2$ as illustrated in Fig. 26.

The solid angle correction for source distance is

$$\Omega = \frac{A}{4\pi R^2} = \frac{\pi\left(r_1^2 - r_2^2\right)}{4\pi R^2} = \frac{r_1^2 - r_2^2}{4R^2} . \quad (5)$$

Since

$$r_2 = r_1\left(1 - \frac{\ell}{\ell + R}\right),$$

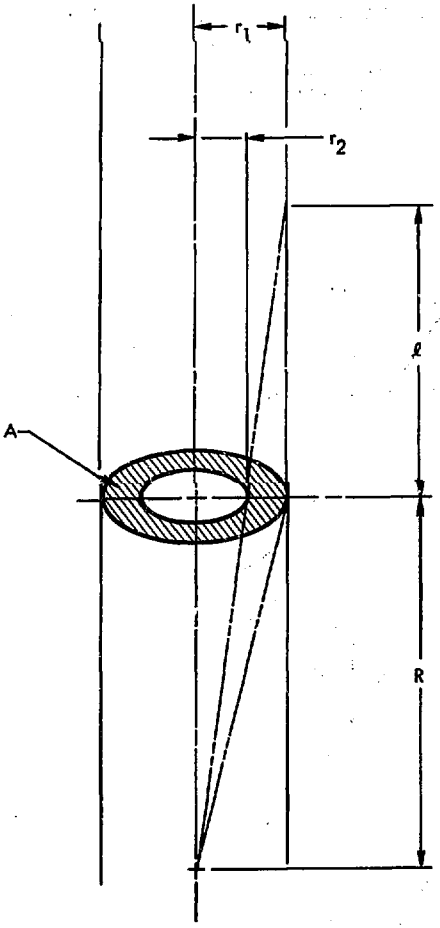

Fig. 26. Solid angle correction factor for uncollimated case.

then

$$\Omega = \frac{r_1^2 - \left[r_1\left(1 - \frac{\ell}{\ell + R}\right)\right]^2}{4R^2} .$$

For a 9-5/8 in. diam pipe and at a source distance of 60 ft and 120 cm length of pipe (as used in SORS)

$$\Omega = \frac{12.2^2 - \left[12.2\left(1 - \frac{120}{120 + 1829}\right)\right]^2}{4(1829)^2}$$

$$= 1.32 \times 10^{-6}. \quad (6)$$

The noise current induced in a short length of protected cable is given by:

$$I_c = S_v \, D \, \Omega \, I_s \, L \quad (7)$$

or

$$\frac{I_c}{I_s L} = S_v \, D \, \Omega$$

where:

I_c = noise current (amps)

S_v = sensitivity (volume) of cable $\left(\frac{\text{A/m}}{\gamma \text{ MeV/cm}^3 \text{ sec}}\right)$

$D = \frac{\gamma \text{ MeV/cm}^3 \text{ sec}}{\text{source photon/sec}}$ in tray (from SORS-G calculations)

Ω = solid angle factor from source as defined by Eq. (5). Note that Ω must use a length, ℓ, consistent with the value used to determine D.

I_s = source intensity (photons/sec)

L = length of cable subject to constant level irradiation (meters)

The current should be calculated for short length of cable, L, because of solid angle variation from the source, and time dependent effects. For a given cable tray protection, the induced current in the cable is assumed to be proportional to the fluence rate calculated outside the pipe wall. Therefore, the fluence rate calculation described in the Fluence Rate Calculations, Uncollimated Case section, page 3, can be expressed in terms of induced noise current per meter for a given cable tray protection. For 7/8 in.

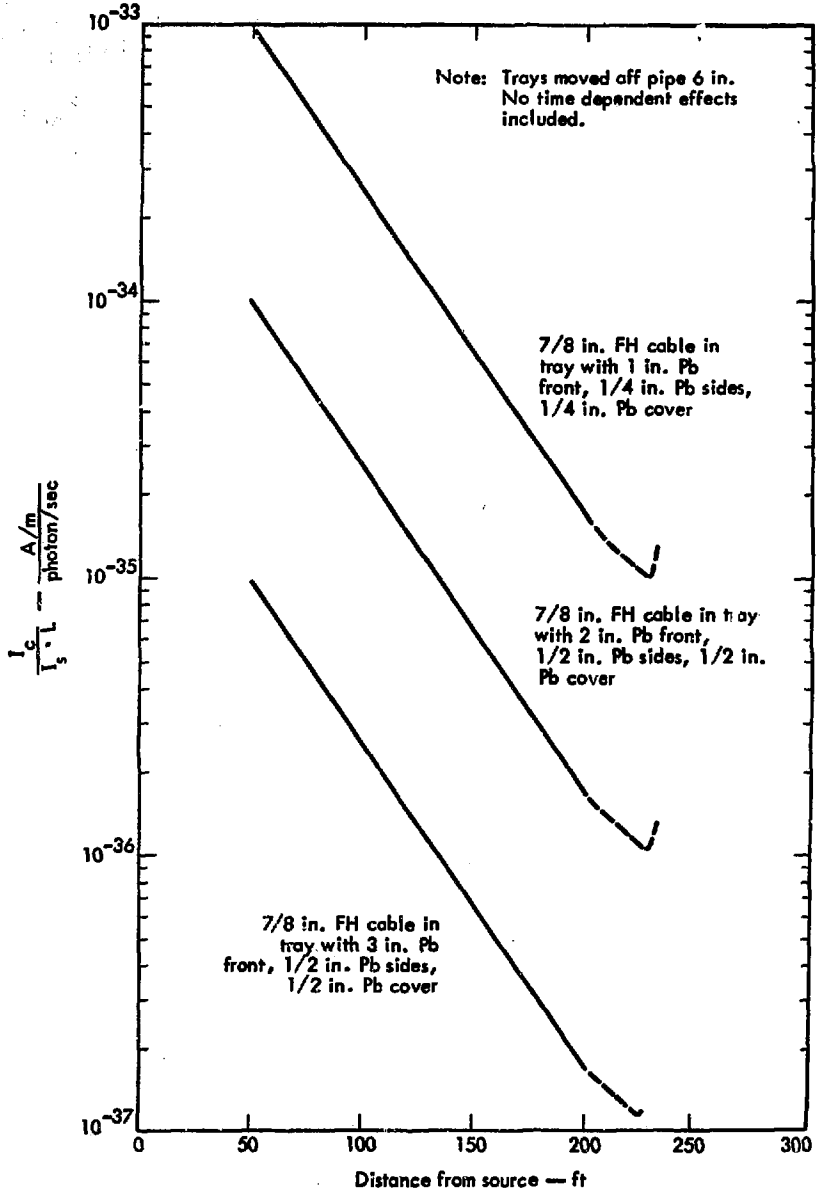

Fig. 27. Induced current in shielded 7/8 in. FH cable.

FH cable, with a sensitivity, S_v, of 2.3×10^{-19} (A/m)/(γ MeV/cm^3 sec), and located inside recommended tray configurations, the value of $I_c/I_s L$ has been plotted as a function of distance from the source in Fig. 27. The experimenter can multiply the value from the graph by the source strength and length of irradiation, L, to determine the induced current at any distance along the pipe. The value of D used for calculating $I_c/I_s L$ was determined from the SORS-G geometry shown in Fig. 9 and was corrected above 200 ft for pinhole scattering by estimating the effect from Fig. 4. (Note that Fig. 4 and Fig. 27 have similar shapes.) For example, with a tray protected by 1 in. Pb front, 1/4 in. Pb sides and 1/4 in. Pb cover, D is 2.51×10^{-9} (γ MeV/cm^3 sec)/(photon/sec) with no pinhole scattering correction. Refer to Table 1 for relative values of D in recommended configurations.

If the trays can be moved farther from the pipe, the current is reduced as illustrated in Fig. 10. Note that Fig. 27 does not include time dependent effects such as described in the Cable Sensitivity and Time Dependent Effects section, page , or source absorption due to filters placed in the pinex LOS. The use of filters will reduce the induced current by their transmission factor. The signal current at the time of induced noise determines a signal-to-noise ratio which can be evaluated by the diagnostic physicist.

COLLIMATED CASE

Collimator Region

An order of magnitude calculation of the induced current in a cable near a collimator can be performed as follows:

$$I_c = I_s \, \psi_s \, S \, \Omega \, L \qquad (8)$$

where

I_c = induced current (A)

I_s = source intensity (photons per sec)

ψ_s = energy fluence rate incident on the cable per source photon per sec

S = cable sensitivity $\left(\frac{\text{A/m}}{\gamma \text{ MeV/cm}^2 \text{ sec}}\right)$

Ω = solid angle subtended

L = length of cable irradiated (m)

The source intensity should be known and corrected for any attenuation between the source and the collimator. ψ_s is the product of ϕ_s and $\bar{E}$, both of which are given in Table 2. The cable sensitivity of some commonly used cables can be obtained from Table 3. The solid angle factor is calculated by:

$$\Omega = \frac{r_o^2 - r_i^2}{4R^2}$$

where r_o is the outer most radius of the collimator struck by direct photons, r_i is the aperture radius, and R is the distance from the source.

For example, using Eq. (8) to calculate the induced current in a cable in the region of a collimator is as follows:

Assume a distance from the source of 100 ft, a 6 in. aperture collimator in 13-3/8 in. o.d. pipe (12.35 in. i.d.) with 7/8 in. FH cable shielded as shown in Fig. 18 with 10 in. standoff. The scattering from the collimator is assumed to be localized along the 4.5 m tray length.

$$\psi_s = \phi_s \bar{E}$$

$$= \left(4.5 \times 10^{-11} \, \frac{\text{photons/cm}^2 \text{ sec}}{\text{source photon/sec}}\right) \times (0.9 \; \gamma \text{ MeV/photon})$$

$$= 4.05 \times 10^{-11} \frac{\gamma \text{ MeV/cm}^2 \text{ sec}}{\text{source photon/sec}}$$

(From Table 2)

$$S = 1.5 \times 10^{-20} \frac{\text{A/m}}{\gamma \text{ MeV/cm}^2 \text{ sec}}$$

(From Table 3)

$$\Omega = \frac{r_o^2 - r_i^2}{4R^2}$$

$$= \frac{(5.67 \text{ in.})^2 - (3.0 \text{ in.})^2}{4(100 \text{ ft} \times 12 \text{ in./ft})^2} = 4.02 \times 10^{-6}$$

Note that r_o is taken as 5.67 in. because of an assumed 1/2 in. of shadowing of the outer region of the collimator from a lower collimator.

$L = 4.5$ m

Substituting into Eq. (8):

$$I_c = I_s (4.05 \times 10^{-11})(1.5 \times 10^{-20}) \times (4.02 \times 10^{-6})(4.5)$$

$$I_c = I_s (1.1 \times 10^{-35}) \frac{\text{A}}{\text{source photon/sec}}$$

A substitution of the source intensity (photons/sec) gives the induced current (A) for this example. This equation gives a conservative result because the peak rate, ψ_s, is assumed to be incident along the entire length, L. If greater accuracy is required, Appendix B contains a more exact form of obtaining I_c from a specific SORS-G calculation. Time related buildup effects discussed in the Cable Sensitivities and Time Dependent Effects section, page 18, are not important around the collimator because of the short distance involved, and thus are not included. The time dependent effects in Appendix B are usually negligible because these times are small in comparison to the source time. Equation (8) was tested with the Arnica Event data which used NHJ-5 cable. The geometry was 5.7 in. aperture collimators located inside a 9-5/8 in. o.d. pipe. Thus, the solid angle subtended by the collimator is about 40% less than the geometry discussed above. The cable trays were made of 3 in. of Pb (1 in. sides and 1/2 in. cover) and stood-off from the pipe only 6 in. Therefore, the Arnica configuration should have received about a factor of 10 greater fluence rate inside the cable trays than the above recommended configuration. No noise signal was discernible, and thus, the less stringent shielding criteria provided adequate cable protection for this situation.

Air Scattering

As previously mentioned in the Fluence Rate Calculations, Collimated Case section, page 10, air scattering contributions need to be considered when the LOS is not evacuated. The induced current due to air scattering can be calculated in a manner similar to the current induced from a collimator region.

$$I_c = I_s \psi_s S \Omega B_t \qquad (9)$$

where B_t represents the time dependent buildup effect discussed in the Cable Sensitivities and Time Dependent Effects section, page 18. (B_t has units of length because it is integrated over the length of the pipe.) A value of ψ_s can be obtained from the tables in the Fluence Rate Calculations, Collimated Case section, page 10, for both the shielded and the unshielded case by multiplying ϕ_s by $\bar{E}$.

Again I_c is believed to be overestimated because of the assumptions. In a recent NTS event, shielding was not used between

collimators, and current was induced in the cables when the LOS lost vacuum. To obtain an estimate of the accuracy of the above equation, I_c was calculated for this event geometry. Since the cables (NHJ-5) between collimators were not shielded (implying a low photon $\bar{E}$ environment), the cable sensitivity obtained by the Pulsed Febitron measurement was used. Also, the time between the peak reaction history signal and the reference voltage (the measured noise voltage at a given time) corresponded to a B_t of approximately 20. The plot of B_t (Fig. 25) includes a solid angle correction, but is normalized to 30 ft. Thus, the solid angle factor, Ω, in the above equation was calculated for 30 ft to reference back to the source. The results of this comparison indicated that the calculated current was about a factor of 10 greater than the measured current.

The Arnica Event provided comparative data for the shielded air scattering environment. The LOS on the Arnica Event also lost vacuum, but the cables were protected by 3 in. Pb trays between the segments of collimator shielding. No noise current was induced, so no factor between the calculated and measured values could be obtained. But even though the Arnica shielding was greater than now recommended, the present recommended shielding is still believed to be greater than necessary for most cases. Thus, results from future events may reduce the shielding recommendations.

Conclusions

Cable protection can be obtained by either collimating the pinex pipe or using continuously shielded cable trays. For the collimated case the shielding arrangement suggested in Fig. 18 can be used around all collimators and the noise current induced near the collimators per source photon per sec will be given by Eq. (8). The air scattering in the collimated case is of sufficient magnitude that we recommend a vacuum LOS requirement and standoff of cables from the pipe. The air scatter contributions per source photon per sec can be estimated from Eq. (9) if no vacuum is used.

To optimally protect cables in the uncollimated geometry the experimenter should determine the required signal-to-noise ratio for his data and determine the location of interaction between his lowest level signal and the highest fluence rate in the pipe. (This will depend on the signal shape and cable used.) The estimated induced noise current as a function of distance from the device can be obtained for several shielding arrangements from Fig. 27. Corrections to the values from Fig. 27 for buildup or different cable sensitivities should be made. Further improvement can be obtained with a Pb filter placed in the pinex pipe and standing the trays farther from the pipe. The effect of the latter is shown in Fig. 10.

Another option available is to increase the detector overlap in regions of the reaction history where it is determined that potential noise problems exist and use less of the detectors' total dynamic range. This may increase the allowable

noise and thus reduce the quantity of shielding required.

Finally, a reduction in the scatter around the pinhole region can be obtained by making the first 2 in. of the pinhole assembly out of Pb. The cable protection in the pinhole region can be done by standard cable trays.

Appendix A
Sensitivity Conversion Factor for 7/8 in. FH Cable

The SORS-G calculation of cable tray design parameters calculated the energy deposited inside the tray with mocked cables. To be conservative in the recommended cable shielding, the sensitivity of Foamflex (FF) cable reported by C. Williams and J. Mead[8] of $1.5 \times 10^{-20} \frac{\text{A/m}}{\gamma\ \text{MeV/cm}^2\ \text{sec}}$ was used to calculate the total energy absorbed by high density foam cable. (The FH and FF cables have been interchangeably used in downhole cable runs.) The cable was assumed to be atomically mixed $Cu_{16}C_{28}H_{56}$ at a density of 2.2 g/cm^3. The energy absorption mass attenuation coefficient for ^{60}Co γ rays (1.25 MeV) is:

$$\text{Cu: } 0.025\ \text{cm}^2/\text{g} \quad \sigma_{Cu} = \frac{63.5}{6.02 \times 10^{23}} (0.025) = 2.6 \times 10^{-24}\ \text{cm}^2$$

$$\text{C: } 0.027\ \text{cm}^2/\text{g} \quad \sigma_{C} = \frac{12}{6.02 \times 10^{23}} (0.027) = 5.4 \times 10^{-25}\ \text{cm}^2$$

$$\text{H: } 0.53\ \text{cm}^2/\text{g} \quad \sigma_{H} = \frac{1}{6.02 \times 10^{23}} (0.052) = 8.67 \times 10^{-26}\ \text{cm}^2$$

$$\sum_a = \frac{\rho N_0 \sigma}{A}$$

$$\sum_a Cu_{16} C_{28} H_{56} = \frac{(2.2)(6.02 \times 10^{23})}{1408} (16\ \sigma_{Cu} + 28\ \sigma_C + 56\ \sigma_H)$$

$$= (9.4 \times 10^{20}) [(41.6 + 15.1 + 4.8) \times 10^{-24}] = 0.058\ \text{cm}^{-1}$$

where:

- σ = microscopic absorption cross section (cm^2)
- $\sum_a$ = macroscopic absorption cross section (cm^{-1})
- ρ = density (g/cm^3)
- N_0 = Avogadro's number (atoms/g-atom)
- A = atomic weight.

The volume sensitivity of a cable, defined in units of $\frac{\text{A/m}}{\gamma\ \text{MeV/cm}^3\ \text{sec}}$ is related to the normal fluence rate sensitivity by

$$S_v = \frac{S}{\sum_a} = \left(1.5 \times 10^{-20} \frac{\text{A/m}}{\gamma\ \text{MeV/cm}^2\ \text{sec}}\right)\left(\frac{1}{0.058\ \text{cm}^{-1}}\right) = 2.6 \times 10^{-19} \frac{\text{A/m}}{\gamma\ \text{MeV/cm}^3\ \text{sec}}.$$

Appendix B
Equation for Determining Induced Cable Noise Current in Collimated Case

The following equation is a more detailed method for determining the induced current in a cable in collimated geometry from SORS-G output. It was not used in the text because it requires very good statistics in order to accurately sum over angles and energy groups in all tally zones.

$$I_c(t) = I_s\, T_m \left\{ \sum_{k=1}^{p} \left[\sum_{i=1}^{n} S_i \sum_{\alpha=1}^{m} b_{i\alpha}\, \phi_{i\alpha} \exp\left(-\mu_i x \cos\alpha\right) \right] + \theta(t) \right\}$$

where

- I_s = source intensity
- T_m = transmission from the source to the collimator
- k,p = k sums over the number of zones, p, that the shielding is divided into
- $\theta(t)$ = phase shift resulting from photon flight time to various zones and cable propagation time between irradiated zones
- i,n = i sums over the number of energy groups, n
- S = cable sensitivity/energy group
- α,m = α sums over the number of angular distribution groups, m
- b = photon buildup factors (including energy spectrum changes)/angular group/energy group
- ϕ = fluence rate/angular group/energy group/zone/source photon/sec
- μ = linear attenuation coefficient/energy group
- x = thickness of tray
- α = angle of photon incidence

References

1. J. Kimlinger, E. F. Plechaty, and J. R. Terrall, SORS Monte Carlo Photon-Transport Code for the CDC 6600, Lawrence Radiation Laboratory, Livermore, Rept. UCRL-50358 (1967).
2. R. Peele and F. C. Maienschein, "Prompt γ Rays From Neutron Fission of U^{235}," Nucl. Sci. Eng. 40, 375 (1970).
3. T. L. Harper, Lawrence Radiation Laboratory, Livermore, private communication (COL 71-21).
4. D. Redhead, Lawrence Radiation Laboratory, Livermore, private communication (UOPE 70-21).
5. B. G. Bennett, G. Burke, and H. L. Beck, Experimental and Theoretical Studies of the Transport of Gamma-Rays Through Slab Shields, Health and Safety Laboratory USAEC, New York, HASL-205 (January 1969).
6. H. Goldstein and J. E. Wilkins, Jr., Calculations of the Penetration of Gamma Rays, Final Report, Nuclear Development Associates, Inc., NYO-3075 (June 30, 1954).
7. T. Rottunda, Lawrence Radiation Laboratory, Livermore, private communication to J. Wobser.
8. C. E. Williams and J. Mead, Effects of Gamma Rays on Coaxial Cables (U), Lawrence Radiation Laboratory, Livermore, Rept. UCRL-7725 (1964) (SRD).

Printed in U.S.A. Available from the National Technical Information Center, National Bureau of Standards, U.S. Department of Commerce, Springfield, Virginia 22151
Price: Printed Copy $3.00; Microfiche $0.65